Fluorescent Phosphorus Dendrimer as a Spectral Nanosensor for Macrophage Polarization and Fate Tracking in Spinal Cord Injury[a]

Antos Shakhbazau,* Manoj Mishra, Tak-Ho Chu, Craig Brideau, Karen Cummins, Shigeki Tsutsui, Dzmitry Shcharbin, Jean-Pierre Majoral, Serge Mignani, Mireille Blanchard-Desce, Maria Bryszewska, V. Wee Yong, Peter K. Stys, Jan van Minnen

Dendrimers and dendriplexes, highly branched synthetic macromolecules, have gained popularity as new tools for a variety of nanomedicine strategies due to their unique structure and properties. We show that fluorescent phosphorus dendrimers are well retained by bone marrow-derived macrophages and exhibit robust spectral shift in its emission in response to polarization conditions. Fluorescence properties of this marker can also assist in identifying macrophage presence and phenotype status at different time points after spinal cord injury. Potential use of a single dendrimer compound as a drug/siRNA carrier and phenotype-specific cell tracer offers new avenues for enhanced cell therapies combined with monitoring of cell fate and function in spinal cord injury.

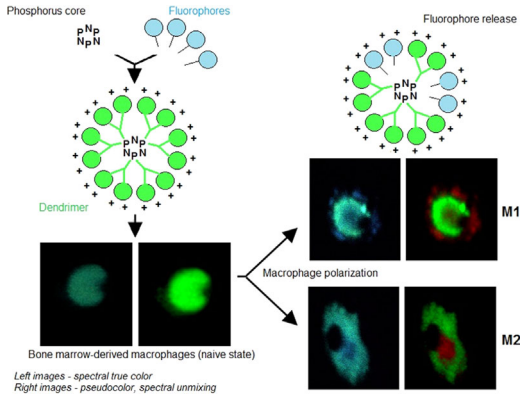

1. Introduction

Dendrimers are synthetic macromolecules of various tailored sizes and composition characterized by a highly branched three-dimensional structure, which endows them with a considerable degree of versatility, multivalency, and tailorable surface functionality, making them useful for many biological applications.[1–5] Chemical structures of dendrimers are precisely defined by their step-by-step synthesis, which allows for fine adjustment of

A. Shakhbazau, M. Mishra, T.-H. Chu, C. Brideau, K. Cummins, S. Tsutsui, V. W. Yong, P. K. Stys, J. van Minnen
Hotchkiss Brain Institute and Cumming School of Medicine, University of Calgary, HRIC 1AA02, 3280 Hospital Drive, NW, T2N4Z6, Calgary, Canada
E-mail: shakhbazau@gmail.com
D. Shcharbin
Institute of Biophysics and Cell Engineering of NASB, Minsk, Belarus

J.-P. Majoral
Laboratoire de Chimie de Coordination, CNRS, Toulouse, France
S. Mignani
Laboratoire de Chimie et de Biochimie Pharmacologiques et Toxicologique, Université Paris Descartes, Paris, France
M. Blanchard-Desce
Institut des Sciences Moléculaires, Université Bordeaux, Talence cedex, France
M. Bryszewska
Department of General Biophysics, Faculty of Biology and Environmental Protection, University of Lodz, Lodz, Poland

[a]**Supporting Information** is available online from the Wiley Online Library or from the author.

© 2015 WILEY-VCH Verlag GmbH & Co. KGaA, Weinheim

DOI: 10.1002/mabi.201500150

16165195, 2015, 11, Downloaded from https://onlinelibrary.wiley.com/doi/10.1002/mabi.201500150 by Universidade De Madeira, Wiley Online Library on [28/02/2024]. See the Terms and Conditions (https://onlinelibrary.wiley.com/terms-and-conditions) on Wiley Online Library for rules of use; OA articles are governed by the applicable Creative Commons License

their general properties and for desired modification of their numerous terminal groups, in turn defining their functionality.[6,7] Dendrimers are represented by multiple subclasses depending on their chemical composition—thus, the subclass of phosphorus dendrimers is defined by the presence of at least one phosphorus atom at each branching point. Branched moieties can be broadly modified to shape the key biochemical properties of dendrimers depending on the desired application, such as surface charge, peptide-based targeting, or fluorescence when fluorophores are incorporated in their structure.[8,1,9] The presence of numerous surface groups (charged or modified as necessary) and a hydrophobic core allows for a high drug payload and multifunctionality, conferring also the ability to transport therapeutic cargos across various cell membranes or biological barriers via cellular internalization.[5] The latter occurs mainly through a clathrin- and caveolae-mediated energy-dependent endocytosis and partly through macropinocytosis.[5,10,11] Cationic dendrimers are then able to escape from endosomes and lysosomes into the cytoplasm via osmotic swelling and membrane rupture. Dendrimers decorated with specific ligands (such as transferrin, lactoferrin, EGF, and others) were successfully used to deliver drugs, peptides, or plasmids across the blood–brain barrier into the CNS (reviewed in).[5] In the present study, we aim to complement and expand the known functions of phosphorus dendrimers by investigating the ability of their fluorescent variety to serve as cell trackers and phenotype sensors in bone marrow (BM)-derived macrophages, with the aim to explore their fate and behavior in a central nervous system injury paradigm.

Earlier reports indicate feasibility of dendrimers in targeting CNS macrophage-like cells, the microglia, in severe injury models.[12,13] Dendrimers were applied as vehicles for CNS-targeted delivery of the anti-inflammatory agent *N*-acetyl-l-cysteine (NAC) in a cerebral palsy model, which resulted in improved myelination, decreased markers of neuroinflammation and oxidative injury, sustained weight, and significant motor improvement.[13] These studies underline the potential of dendrimer-based targeting in future therapies for neurologic diseases and injuries. Dendrimers are also being tested in preclinical research for cancer treatment, anti-inflammation, and targeted delivery.[13,14] Certain modifications of phosphorus dendrimers were shown to inhibit alpha-synuclein fibrillation (related to Parkinson's disease),[15] interfere with the $A\beta_{1-28}$ fragment and MAP-Tau protein aggregation processes (related to the onset and development of Alzheimer's disease),[16] and to modulate activation of monocytes;[17–19] these dendrimer species possess remarkable anti-inflammatory properties, as demonstrated in rodent models of uveitis[20] and experimental arthritis.[14] We have previously reported the properties of phosphorus dendrimers as gene and siRNA transfection reagents in stem cells and other cell types.[21–23] Dendrimers also emerged as potent antibacterial agents,[24] regulators of natural killer cells,[25] and in numerous other applications.[4,26–28]

We and others have previously shown that dendrimers can be used for modification of candidate cell types for cell therapy applications.[6,29–31] Cell therapy is one approach toward treatment of central and peripheral nervous system disorders, with many cell types shown to improve recovery in trauma and disease paradigms.[32–36] These cell types include, but are not limited to, stem cells of various origins, for which differentiation or trans-differentiation protocols were developed.[37–40] Macrophages, the phagocytic cells of the immune system, have also been reported as potent agents for cell therapy in CNS trauma.[41,42] Blood-borne macrophages activated ex vivo by exposure to peripheral nerve[34] or skin[43] fragments remarkably improved functional regeneration after severe spinal cord injury, an approach culminating in clinical trials in human patients.[35] BM-derived macrophages were also shown to be potent actors in chronic CNS disorders,[44,45] e.g., restricting senile plaque formation in Alzheimer's disease[46]and arresting pathology in a murine model of X-linked autism spectrum disorder.[47] Macrophages could be further modified to act as vehicles for gene or drug delivery across the blood–brain barrier (BBB), presenting a rationale for the development of novel therapeutic strategies.[48–50]

Macrophages have long been seen as one of the critical effectors in the course of CNS injuries and diseases.[44,45,51,52] Functional phenotypes of macrophages and microglia have been traditionally divided into the M1 (pro-inflammatory, phagocytic, and cytotoxic) and M2 (anti-inflammatory, regulatory, and reparative), subdivided lately into further subclasses and intermediate states.[53–57] Each of the "extreme" phenotypes is characterized by upregulation of specific genes (e.g., TNF-α and iNOS for M1, arginase-1 and CD206 for M2) and plays a distinct role in different settings of disease or injury.[53,54,56] Recent work provides strong evidence that macrophages show a remarkable phenotypic plasticity and can seemingly adopt a spectrum of polarization states depending on environmental signals.[44,54,55,58] In CNS injury and disease, macrophages also exhibit context-dependent pro-inflammatory M1 activation and/or anti-inflammatory and neuroprotective M2 function.[44,59,60] The role and potential of macrophages, alone or with modifying agents, in CNS recovery is currently of significant academic and clinical interest.[44,52,61]

The purpose of the current study is to analyze the ability of phosphorus dendrimers to target macrophages and serve as fluorescent tracers under in vitro and in vivo activation conditions. Relying on the ability of

© 2015 WILEY-VCH Verlag GmbH & Co. KGaA, Weinheim

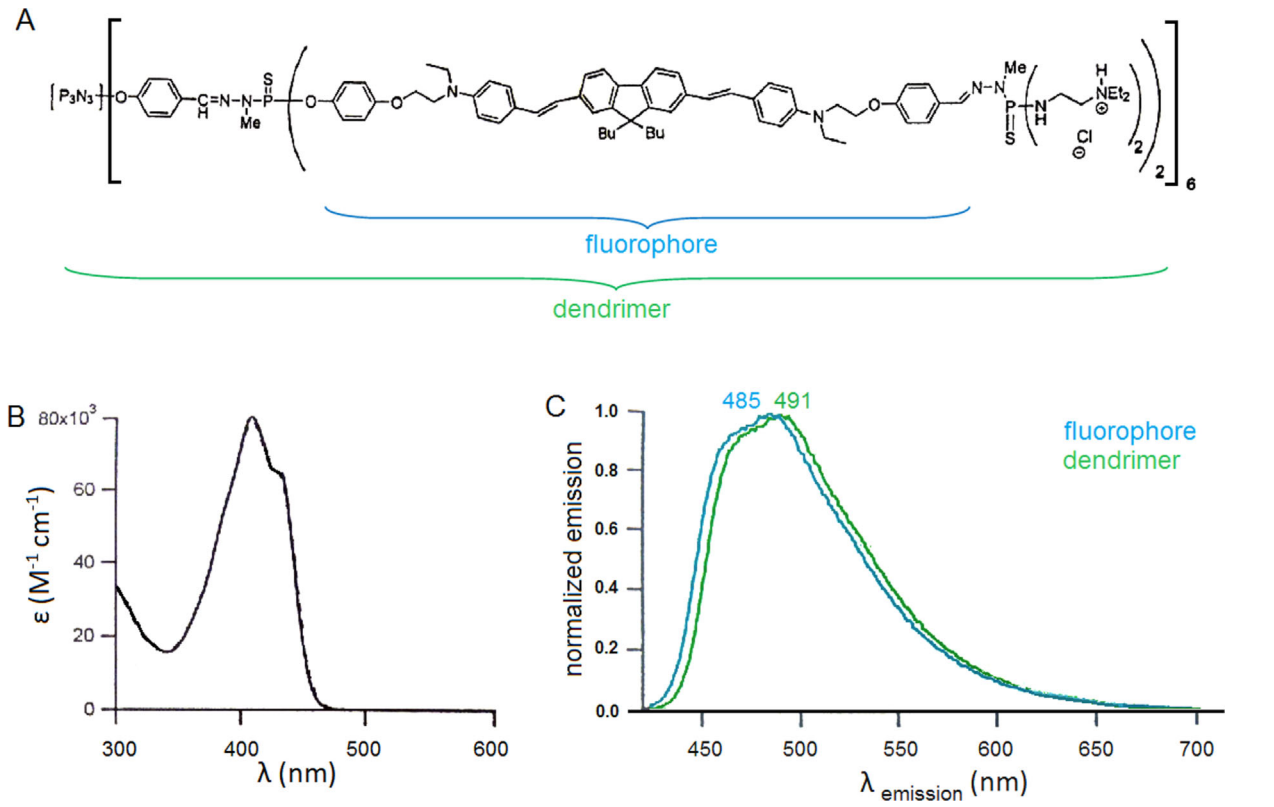

Figure 1. Fluorescent phosphorus-based dendrimer: (A) chemical formula; (B) dendrimer excitation spectrum; and (C) normalized emission spectra of dendrimer and its constituent fluorophore (λ_{max} in tetrahydrofuran (THF).

our novel synthetic fluorescent fluorophore to change its spectral signature upon assembly into the dendrimer complex, we hypothesized that the microenvironment-specific dendrimer structure alteration will lead to context-dependent fluorophore release, shifting its spectrum and thus creating a spectral imaging sensor. In the present study, we have tested this bio-imaging system to trace the changes in physiological status of the bone marrow-derived macrophages in both in vitro and in vivo polarization conditions.

2. Materials and Methods

2.1. Fluorescent Phosphorus Dendrimer

Our bio-imaging tracer for murine BM-derived macrophages was a modified phosphorus-based dendrimer (MW 16 348.61 Da), harboring 12 fluorophores and 24 cationic groups on the near spherical surface of its molecule. The fluorophore (Figure 1A) was prepared and assembled on the phosphorus dendrimer according to the principles described earlier.[8,9] Briefly, the dissymmetric fluorophore (Suppl. Figure 1A) bearing two functional moieties (benzaldehyde and phenol) in the extremes was obtained as single (*E*,*E*)-stereoisomers, by means of twofold-Heck reaction between the iodinated moieties (Suppl. Figure 1B,C) and the *bis*-vinyl fluorene core in one pot reaction, then following saponification leading to the corresponding fluorophore (Suppl. Figure 1A). The fluorophore was then introduced on the surface of a phosphorus dendrimer of generation 1 harboring 6 terminal $P(S)Cl_2$ units via nucleophilic substitution involving the phenolic group of dissymmetric fluorophore, thus allowing to form the corresponding dendrimer bearing fluorophore units with aldehyde terminal groups. Condensation of these aldehyde groups with the monomethylhydrazino-dichloro-thiophosphine $H_2NN(CH_3)P(S)Cl_2$ followed by nucleophilic substitution reaction with the diamine $H_2N(CH_2)_2$ NEt_2 led to the final fluorescent phosphorus-based dendrimer. The complete structure of the dendrimer, as well as its excitation and normalized emission spectra are shown in Figure 1.

2.2. Bone Marrow Macrophage Isolation and Culture

Bone marrow was flushed from femurs of C57BL/6 mice using a PBS-filled syringe and passed through a cell strainer; cells were centrifuged at 1 500 rpm for 5 min at 4 °C and

© 2015 WILEY-VCH Verlag GmbH & Co. KGaA, Weinheim

16165195, 2015, 11, Downloaded from https://onlinelibrary.wiley.com/doi/10.1002/mabi.201500150 by Universidade De Madeira, Wiley Online Library on [28/02/2024]. See the Terms and Conditions (https://onlinelibrary.wiley.com/terms-and-conditions) on Wiley Online Library for rules of use; OA articles are governed by the applicable Creative Commons License

16165195, 2015, 11, Downloaded from https://onlinelibrary.wiley.com/doi/10.1002/mabi.201500150 by Universidade De Madeira, Wiley Online Library on [28/02/2024]. See the Terms and Conditions (https://onlinelibrary.wiley.com/terms-and-conditions) on Wiley Online Library for rules of use; OA articles are governed by the applicable Creative Commons License

seeded at 2×10^6 cells · mL^{-1} in 90 mm sterile Petri dishes in DMEM supplemented with 10% heat-inactivated FBS, 1% penicillin/streptomycin (Invitrogen), and 15% L929-cell conditioned medium containing macrophage colony stimulating factor (M-CSF). Macrophage polarization was performed using cytokine cocktails known to generate M1 and M2 phenotypes.[54–56] M1 polarization cocktail contained 100 ng · mL^{-1} lipopolysaccharides (LPS) and 100 ng · mL^{-1} IFN-γ in DMEM, and M2 polarization cocktail contained 20 ng · mL^{-1} IL-4 and 10 ng · mL^{-1} IL-13 in DMEM.

2.3. Quantitative Real-Time PCR

BM-derived macrophages were polarized for 10 h and the samples for RNA isolation were harvested in TRIzol reagent (Invitrogen, Carlsbad, CA) and stored at −80 °C before use. RNA was extracted using the RNeasy Mini Kit columns (Qiagen, Mississauga, ON, Canada), treated with DNase (Promega, Madison, WI), and reverse transcribed using Superscript II Reverse Transcriptase (Invitrogen). The resulting cDNA served as a template for qPCR using the Bio-Rad iCycler detection system (Bio-Rad, Hercules, CA) and 2× SYBR Green Master Mix (Qiagen). Primers for iNOS, Arg-1 and GAPDH were purchased from Qiagen (10× QuantiTect Primer Assay), and used according to the manufacturer's instructions. Expression of gene transcripts was normalized against the housekeeping gene GAPDH.

2.4. Cell Exposure to Dendrimers

For dendrimer loading studies, macrophages were cultured in DMEM supplemented with 10% heat-inactivated FBS, and 1% penicillin/streptomycin (Invitrogen) to maintain naïve state (D10); 15% L929-cell conditioned medium was added to induce macrophage differentiation via M-CSF (conditioned differentiation medium hereafter referred to as Dcon, or D10 w/M-CSF), M1 or M2 serum-free cocktails were added to induce polarization in vitro 2 d before the dendrimer exposure. Dendrimer was initially dissolved in DMSO to a concentration of 8.22 mg · mL^{-1} (theoretical correspondence to a molar concentration of 0.5 mM); working dilutions were next made in 150 mM NaCl which was added to cell culture as 10% of medium v/v to achieve final concentrations of 1.65, 16.5, and 165 μg · mL^{-1} (theoretical correspondence to molar concentrations of 0.1, 1 and 10 μM). Cells were observed under a laser-scanning spectral confocal microscope (C1si, Nikon). Spectral unmixing was used to assist in segregating cells into spectrally shifted versus spectrally unchanged phenotype, while the extent of hypsochromic (blue) shift was assessed by comparing multiple regions of interest (ROIs) in blue-shifted cell areas with the reference ROIs in the rest of green-fluorescing cytoplasm.

2.5. Spinal Cord Injury

C57BL/6 mice were anaesthetized with isoflurane (99.9% Halocarbon Laboratories, River Edge, NJ, USA) and a partial laminectomy was made at the 10th thoracic vertebral level. Pain control was provided by means of i.p. administration of buprenorphine. A moderate contusion injury (65 kDynes force) was made on the exposed spinal cord using the Infinite Horizons impactor device, as described.[62] The wound was closed in layers, and the impact effect was confirmed the next day by BMS locomotion test. Manual bladder expression was done twice a day, and the mice were closely monitored for urinary tract infection. The protocol was approved and monitored by the University of Calgary Animal Care Committee and adhered strictly to guidelines set by the Canadian Council on Animal Care.

2.6. Cell Injections

Macrophages were loaded with 1 μM dendrimer in vitro (Dcon medium, 24 h) as described above, harvested by trypsin incubation, washed in HBSS and resuspended in culture media at 10^4 cells · μl^{-1}. To monitor cell delivery, 0.1% FastGreen was added to the cell suspension before injection. Injections were made in the subarachnoid space immediately after injury using 5 μl Hamilton syringe with a 30 gauge needle caudal to the injury site, or intravenously into the tail vein, to a total of 10^5 cells/animal. In separate experiments, dendrimer solution in 150 mM NaCl was injected directly into the tail vein to achieve blood concentration of ≈1 μM. Animals were maintained in a temperature and humidity controlled environment with a 12-h light/dark cycle. Food (Purina, Mississauga, ON, Canada) and water were available ad libitum.

2.7. Cell and Tissue Analysis

Mice were sacrificed at week 1 or week 2 time points after injury under deep anaesthesia with transcardial perfusion with 4% paraformaldehyde (PFA) in PBS. Spinal cords of 10 mm length centered on the epicenter of injury were carefully excised, post-fixed in 4% PFA, cryoprotected in 30% sucrose, embedded into OCT and sectioned on a cryostat (Leica) at 25 μm. Some spinal cords were also assessed as a whole (with dura removed) with an epifluorescence Nikon A1 microscope before sectioning. Dendrimer fluorescence in injected cells was excited at 408 nm, nuclei were counterstained with DAPI (1:5,000) in some slides, and myelin was stained with lipophilic

© 2015 WILEY-VCH Verlag GmbH & Co. KGaA, Weinheim

dye Nile Red (25 μM). Samples were observed under a laser-scanning spectral confocal microscope (C1si or A1, Nikon).

2.8. Data Analysis

Spectral data were analyzed using EZ-C1 software (Nikon), and spectral distributions were analyzed using methods developed by ST and PKS. Differences between groups were analyzed using a one-way ANOVA, statistical significance was accepted at $P < 0.05$ for pairwise comparisons. All results are presented as the mean ± SEM, and denoted according to the following: * $P < 0.05$; ** $P < 0.01$; *** $P < 0.001$.

3. Results

We first assessed dendrimer properties as a cell targeting probe in vitro by investigating dendrimer uptake by macrophages at different concentrations, and its stability and potential toxicity. We exposed macrophages to the logarithmic range of dendrimer concentrations of 1.65, 16.5, and 165 μg · mL^{-1} (theoretical correspondence to molar concentrations of 0.1, 1, and 10 μM) either in D10 or Dcon media. At each concentration, macrophages were able to take up dendrimer and emit bright fluorescence when excited with 408, 457, or 488 nm lasers in both naïve and differentiating states (Figure 2). 165 μg/mL^{-1} appeared to elicit cytotoxic effects (data not shown), an effect not observed when DMSO alone was added to the culture medium. 1.65 μg · mL^{-1} was suboptimal for effective uptake, with 25–30% efficiency (Figure 2, Suppl. Figure 2), while at 16.5 μg · mL^{-1} virtually all of exposed macrophages were brightly positive (Suppl. Figure 2). At both 1.65 and 16.5 μg · mL^{-1}, macrophages were viable and able to maintain bright fluorescence for at least 5 weeks in culture (Figure 2C). 1.65 μg · mL^{-1}-exposed macrophages in M-CSF containing medium, but not in D10, showed some decline in number of positive cells at later time points, probably due to tracer dilution after cell divisions, while at 16.5 μg · mL^{-1} cell divisions caused reduction in fluorescence intensity but all daughter cells were still positive. Dendrimer fluorescence maximum after macrophage uptake was at ≈505 nm, somewhat red-shifted compared to the measurements in THF solution (Figure 1C), possibly due to increased intramolecular charge transfer between the dendrimer core and periphery in a more polar intracellular environment.[63] The dendrimer was evenly distributed in the cytoplasm, with some fragmentation appearing at later time points after cell divisions, while nuclei were effectively protected from dendrimer influx (Figure 3A, E and 4C, D).

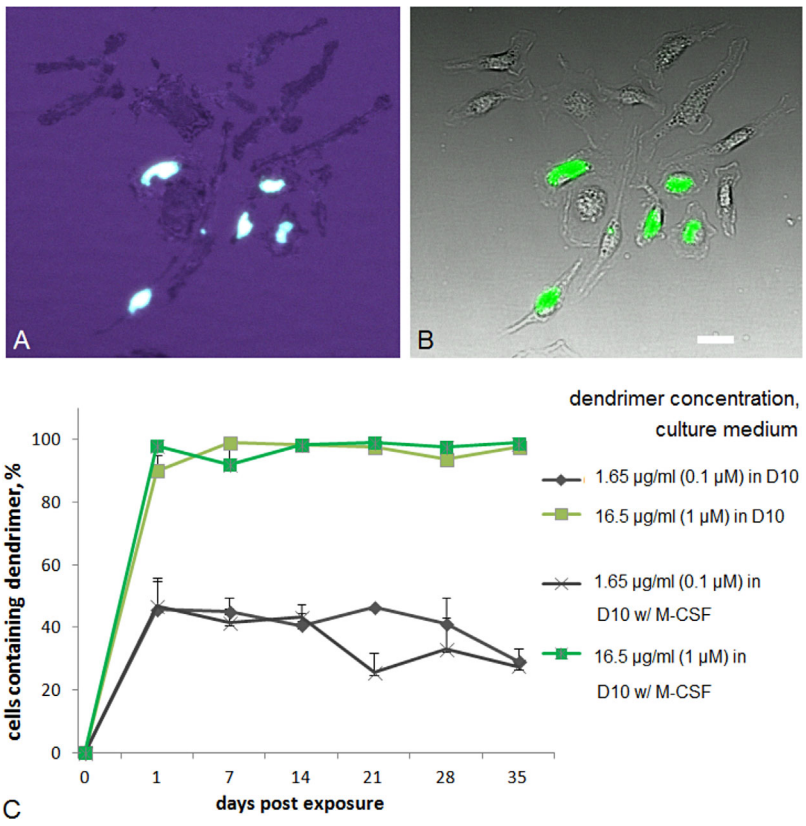

Figure 2. Dendrimer uptake and retention by BM-derived murine macrophages: (A) spectral true color image of dendrimer uptake by the macrophages in vitro, 1.65 μg · mL^{-1} concentration, 408 nm laser; (B) pseudocolor of dendrimer fluorescence in A overlaid on differential interference contrast (DIC) image (scale bar 20 μm); and (C) long-term retention of dendrimer by macrophages in standard (DMEM + 10% FBS) and differentiation (M-CSF containing) media. Dendrimer concentrations ≤16.5 μg · mL^{-1} showed no long term toxicity.

We then assessed dendrimer fluorescence properties in media known to induce macrophage polarization toward either pro-inflammatory (classical, M1) or protective (alternative,M2) phenotype. Macrophage polarization was performed according the published protocols,[54–56] and resulting M1 and M2 phenotypes were confirmed by qPCR for selective expression of phenotype-specific genes iNOS and Arg-1 (Suppl. Figure 3). In each cocktail, macrophages retained their ability to take up and maintain dendrimer molecules, however their fluorescence emission profiles demonstrated remarkable subcellular variations, generating distinct polarization-specific spectral phenotypes (Figure 3,4). In M1 cocktail, intracellular dendrimer in

© 2015 WILEY-VCH Verlag GmbH & Co. KGaA, Weinheim

16165195, 2015, 11, Downloaded from https://onlinelibrary.wiley.com/doi/10.1002/mabi.201500150 by Universidade De Madeira, Wiley Online Library on [28/02/2024]. See the Terms and Conditions (https://onlinelibrary.wiley.com/terms-and-conditions) on Wiley Online Library for rules of use; OA articles are governed by the applicable Creative Commons License

16165195, 2015, 11, Downloaded from https://onlinelibrary.wiley.com/doi/10.1002/mabi.201500150 by Universidade De Madeira, Wiley Online Library on [28/02/2024]. See the Terms and Conditions (https://onlinelibrary.wiley.com/terms-and-conditions) on Wiley Online Library for rules of use; OA articles are governed by the applicable Creative Commons License

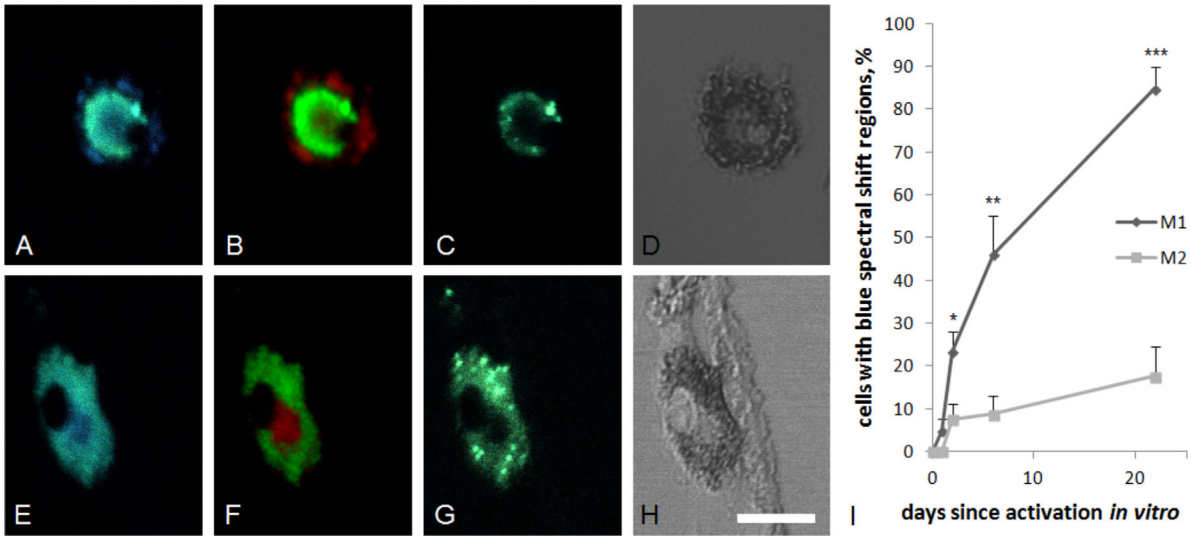

Figure 3. Spectral shift of dendrimer fluorescence in M1-activated (A–D) and M2-activated (E–H) macrophages in vitro. (A,E) spectral images of activated macrophages under 408 nm laser, true color; (B,F) spectral unmixing of images in A and E, pseudocolors here and below represent blue-shifted regions as red, and reference cytoplasm as green; (C,G) spectral images under 457 nm laser, true color, reveals more morphological detail of intracellular dendrimer localization, but is unable to detect blue-shifted regions (cf also Suppl. Figure 4); (D,H) DIC images (scale bar 20 μm); and (I) timeline of blue spectral shift in dendrimer fluorescence under two polarization regimens.

most cells (Figure 3I) was segregated into regions showing hypsochromic (blue) spectral shift in fluorescence (Figure 3A, pseudocolored red in Figure 3B), corresponding to an emission maximum of a fluorophore released from the dendrimer structure (Figure 1). This change was present as distinct regions of blue-shifted fluorescence distributed in the periphery of cell cytoplasm, the rest of which retained green fluorescence similar to D10 culture conditions and was used for reference. In a significantly smaller (Figure 3I) proportion of M2-exposed macrophages, blue-shifted areas also appeared but were mostly localized in perinuclear areas (Figure 3E), in contrast with peripheral distribution in M1-activated cells (Figure 3A,E). To assess dendrimer emission lability in view of current paradigms on macrophage plasticity,[58] we inverted the activation cocktails (M1 to M2, or M2 to M1), which indeed induced some of macrophages loaded with dendrimer in the first cocktail to change their spectral phenotype in response to a new set of stimulating factors ($6.7 \pm 3.9\%$ of M2-like cells appeared by day 2 after M1 to M2 inversion, and $19.4 \pm 6.4\%$ of M1-like cells were seen in M2 to M1 setting).

The range of blue shift was also markedly greater in M1-activated macrophages (Figure 4A,B)—an average 28 ± 2 nm, versus 17 ± 2 nm in M2-activated cells. In view of earlier findings on the role of M-CSF in stimulating M2-type differentiation,[64] we have also examined spectral properties of macrophages in M-CSF-containing differentiation medium (Dcon). Indeed, perinuclear spectral shift was observed in a subset of dendrimer-loaded cells ($22.6 \pm 8\%$ at 3 weeks time point), with a phenotype of cells with perinuclear blue-shifted regions closely resembling those obtained in M2 polarization cocktail (Figure 4C, D). Average extent of spectral shift in M-CSF containing differentiation medium was also indistinguishable from M2 macrophages—17 ± 3 nm (Figure 4B).

Our next aim was to recapitulate our observations on stability and spectral properties of dendrimers in macrophages in vivo after spinal cord contusion injury (SCI). Although intracellular dendrimer continuity was distorted due to swelling or cell morphology changes in a 3D microenvironment, dendrimer-loaded cells were readily detectable at both 1 and 2 week time points after subarachnoid injections. Implanted macrophages were easily found in the injured spinal cords, while presence of fluorescent cells after injections into sham-operated cords was minimal (Figure 5). Labeled macrophages were also clearly detectable using epifluorescence (under A1 Nikon microscope) in the whole fixed spinal cords prior to cryosectioning, making the fluorescent dendrimer a promising candidate for live longitudinal imaging. Dendrimer-positive macrophages were also observed in animals' lungs after systemic injections of dendrimer-loaded macrophages and dendrimer solution, evidence for in vivo dendrimer uptake by host hematogenous phagocytes (Suppl. Figure 4). Dendrimer signal after systemic injections was also present in spleens (Suppl. Figure 5), but not in the injured spinal cords, suggesting the need for further optimization of concentrations and possibly a more severe injury model.

© 2015 WILEY-VCH Verlag GmbH & Co. KGaA, Weinheim

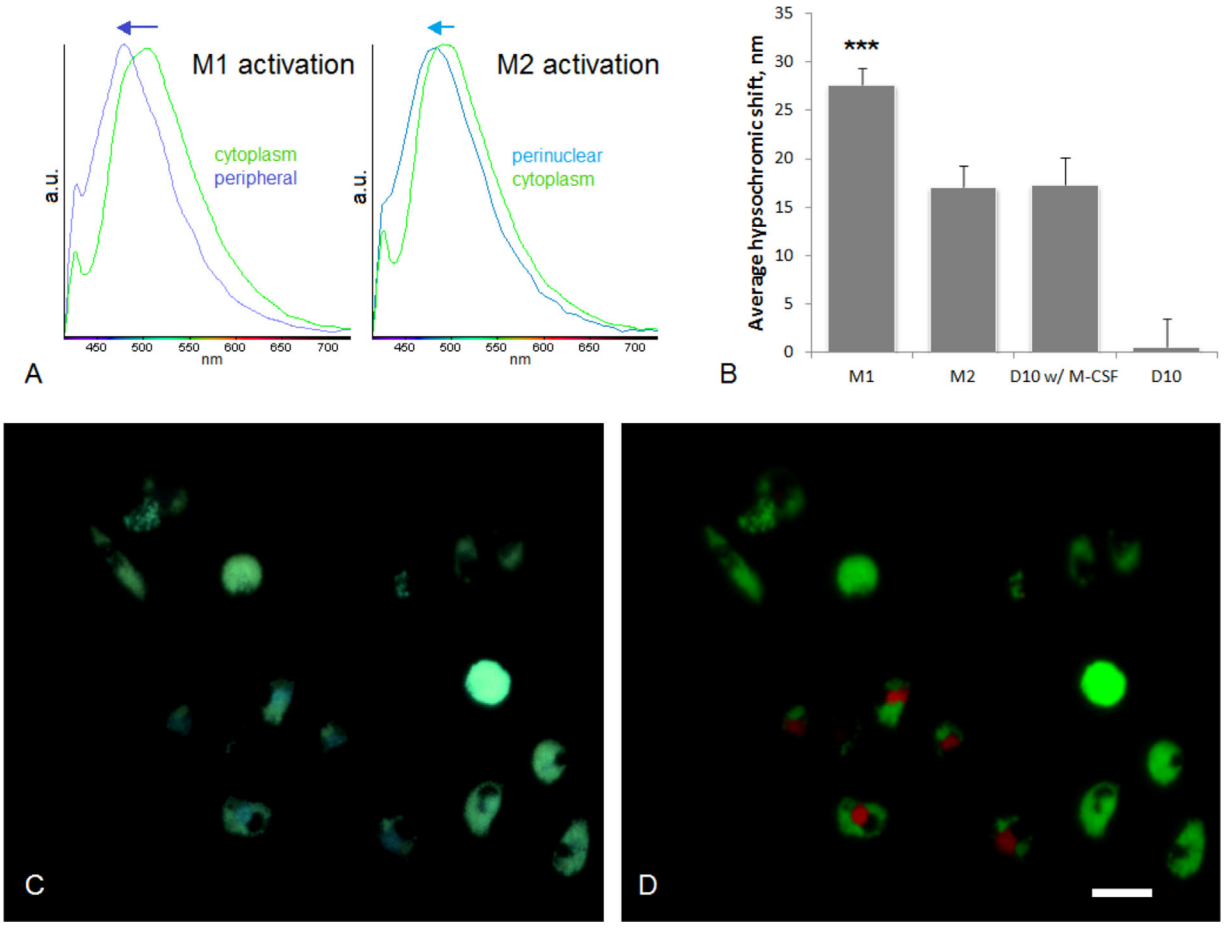

Figure 4. Variation in spectral shift in dendrimer fluorescence under different macrophage culture conditions. (A) spectra of blue versus green regions in M1- and M2-activated macrophages; (B) range of blue spectral shift in macrophages after M1- and M2-activation, differentiation (D10 with M-CSF) and control culture (D10), *** difference significant, $P < 0.001$; (C) spectral shift in macrophages after 3 weeks in differentiation medium (D10 with M-CSF), true color (408 nm laser), a potential sign of spontaneous M2 polarization; and (D) spectral unmixing of the image in C, pseudocolor. Scale bar 20 μm.

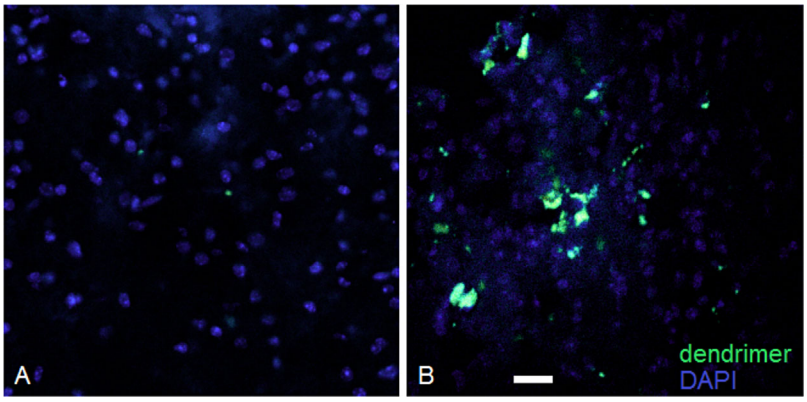

Figure 5. Retention of transplanted dendrimer-loaded macrophages in mouse spinal cord after subarachnoid cell injection (spectral true color, 408 nm laser). (A) sham injury; (B) spinal cord contusion injury (scale bar 20 μm).

We then focused on macrophage phenotypes in the spinal cord after subarachnoid injections. In line with our in vitro observations, a subset of macrophages during the peak of the inflammatory phase (1 week after injury) showed the presence of blue-shifted peripheral granules, although the scale of this phenomenon was more modest: 42.2 ± 11.3% of implanted cells observed in spinal cord sections at week 1 (Figure 6A,B) exhibit peripheral regions with spectral shift in dendrimer fluorescence (28 ± 3 nm, Figure 6C) typical for M1 but not M2 activation in culture.

At the 2 week time point, corresponding to the phase of attempted functional

© 2015 WILEY-VCH Verlag GmbH & Co. KGaA, Weinheim

16165195, 2015, 11, Downloaded from https://onlinelibrary.wiley.com/doi/10.1002/mabi.201500150 by Universidade De Madeira, Wiley Online Library on [28/02/2024]. See the Terms and Conditions (https://onlinelibrary.wiley.com/terms-and-conditions) on Wiley Online Library for rules of use; OA articles are governed by the applicable Creative Commons License

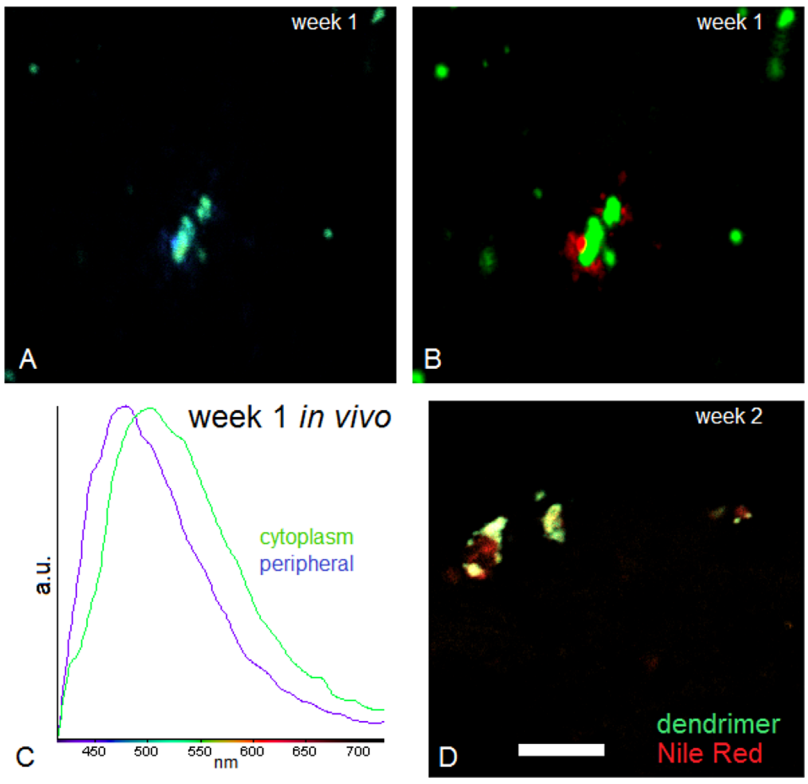

Figure 6. Properties of transplanted dendrimer-loaded macrophages at different stages of regenerative response after contusion injury. (A) macrophages demonstrate peripheral blue shift in the inflammatory phase (1 week after injury/subarachnoid cell injection, spectral true color, 408 nm laser); (B) spectral unmixing of the image in A, pseudocolor; (C) spectral phenotype of macrophages in the inflammatory phase of SCI (1 week in vivo) recapitulates M1 activation in vitro; and (D) macrophages at 2 weeks after injury/subarachnoid cell injection uptake myelin debris (stained with Nile Red dye), switching to protective phenotype in the recovery phase (spectral true colors, 408/561 nm lasers). Scale bar 20 μm.

recovery, M1-associated hypsochromic regions were no longer observed. This is in agreement with existing data on macrophage polarization switch from pro-inflammatory M1 to intermediate or protective M2 phenotype upon myelin debris phagocytosis[65,60] (confirmed by Nile Red-positive fragment uptake by macrophages, Figure 6D). Due to a different morphological context in vivo, we were unable to detect clearly delineated perinuclear blue-shifted areas in macrophages at the 2 week time point, analogous to M2 activation in vitro (Figure 3E, 4C). Spectral variations were detected in a small (<5%) proportion of cells (cf Figure 3I for the proportion of blue-shifted cells in M2 condition), and the spectral shift, if any, was closer to the in vitro M2 phenotype (18 ± 3 nm). Presented data also suggest that dendrimer load does not impair the ability of macrophages to survive through the different phases of SCI and maintain their key function of myelin debris phagocytosis (Figure 6).

We next used an unbiased spectral analysis technique to analyze spectral heterogeneity of dendrimer fluorescence in macrophages in the above mentioned in vitro and in vivo conditions. Figure 7 provides representative bar graphs of dendrimer/fluorophore spectral distribution in pro-inflammatory (M1 activation in vitro, and early time point after SCI) and anti-inflammatory (M2 activation in vitro) settings.

Spectral heterogeneity in the spectral analysis is represented in the form of pixel distribution plots according to their index—the spectral proximity of every pixel to each of the two reference (bracketing) spectra. The bracketing spectra were selected from the unmixed M1 activation image, since this condition represents the highest degree of spectral variability (Figure 4B). An index of 0 is associated with the reference cytoplasm of the dendrimer-loaded macrophage (Figure 4), while an index of 1 is associated with the most blue-shifted areas in M1-polarized macrophages. Continuity of index values on this scale was then divided into quintiles, with index 0 included in the first quintile and index 1 included in the fifth quintile, and a percentage of pixels falling into each quintile was summarized in a bar graph. Low-intensity pixels in the spectral images were excluded from analysis because of increasing spectral uncertainty due to poor signal-to-noise. Graphs in Figure 7, corresponding to the macrophages from Figure 3 and 6, present in refined digital form our data on different in vitro conditions and in vivo environment-dependent phenotypic plasticity. Figure 7 adds to our notion that both abundance and range of dendrimer spectral variability are distinct in M1 and M2 macrophage activation regimens in vitro and are well recapitulated in respective phases of macrophage responses in SCI.

4. Discussion

Novel imaging techniques to monitor inflammatory and regenerative responses in the nervous system are gaining appreciation in both research and clinical applications.[66] Fluorescent cell tracers, mostly designed to bind cell membranes or proteins, have emerged of late as powerful tools to study cell physiology, proliferation, differentiation,

© 2015 WILEY-VCH Verlag GmbH & Co. KGaA, Weinheim

16165195, 2015, 11, Downloaded from https://onlinelibrary.wiley.com/doi/10.1002/mabi.201500150 by Universidade De Madeira, Wiley Online Library on [28/02/2024]. See the Terms and Conditions (https://onlinelibrary.wiley.com/terms-and-conditions) on Wiley Online Library for rules of use; OA articles are governed by the applicable Creative Commons License

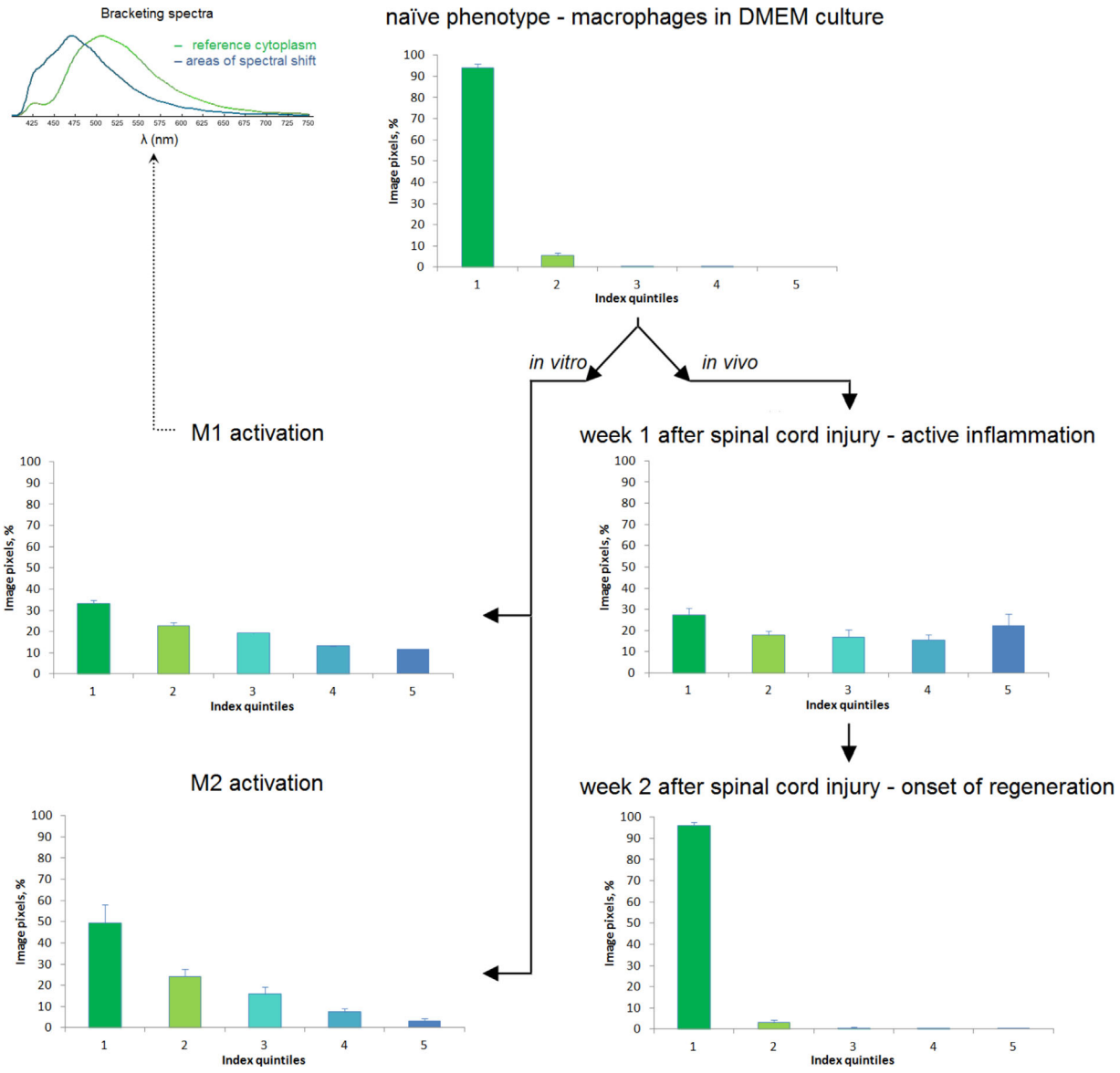

Figure 7. Spectral analysis of phosphorus dendrimer fluorescence patterns in murine BM-derived macrophages.

migration, survival, and many other processes in vitro and in vivo using flow cytometry and a variety of imaging techniques.[36,67,68] Dendrimer-based approaches have also made significant advances in bio-imaging.[1,5] Dendrimers complexed with gadolinium Gd(III) produced a dual modality imaging agent for both magnetic resonance and fluorescence imaging.[69] Dendrimer-based nanoprobes labeled with MR/optical reporters and targeting peptides (RGDyK and angiopep-2) efficiently crossed the intact BBB in normal mice, and precisely delineated the boundary of glioblastoma xenografts.[70] Dendrimer-based sodium-sensitive nanoprobes showed high stability and sodium sensitivity and selectivity when used for ion imaging in neurons in live brain tissue.[71] Moreover, dendrimers built with the photocleavable linkers may allow for light-controlled drug release via photochemical internalization, which was for instance used to completely inhibit cancer cell growth in a UV-light-controlled manner.[72] Fluorescent-labeled PAMAM dendrimers were localized in activated microglia and astrocytes following both subarachnoid[12] and systemic intravenous dendriplex administration, with no effects on renal and hepatic function.[13]

We have applied the new fluorescent subtype of phosphorus dendrimer, a class of molecules increasingly used in many biomedical applications,[14,15,17,23] to target and trace the fates of BM-derived macrophages. Robust uptake and stability of fluorescent phosphorus dendrimer

© 2015 WILEY-VCH Verlag GmbH & Co. KGaA, Weinheim

16165195, 2015, 11, Downloaded from https://onlinelibrary.wiley.com/doi/10.1002/mabi.201500150 by Universidade De Madeira, Wiley Online Library on [28/02/2024]. See the Terms and Conditions (https://onlinelibrary.wiley.com/terms-and-conditions) on Wiley Online Library for rules of use; OA articles are governed by the applicable Creative Commons License

16165195, 2015, 11, Downloaded from https://onlinelibrary.wiley.com/doi/10.1002/mabi.201500150 by Universidade De Madeira, Wiley Online Library on [28/02/2024]. See the Terms and Conditions (https://onlinelibrary.wiley.com/terms-and-conditions) on Wiley Online Library for rules of use; OA articles are governed by the applicable Creative Commons License

in macrophages is a contrast to our previous studies, where phosphorus-based dendrimers were used for non-viral gene delivery via GFP-encoding plasmids and showed inferior efficiency compared to other types of dendrimers.[22] Phosphorus dendrimers were however shown to be effective carriers for drug and siRNA delivery.[21,23] This difference is well explained by the observed pattern of intracellular distribution of phosphorus dendrimer, with effective and long-term retention in cytoplasm but virtually no access to the cell nucleus, which is imperative for transgene expression (Figure 3A,E and 4C,D). Although, further studies will be required to determine the fesibility of each dendrimer variety for cargo loading and fluorescence retention properties, our observations suggest a good prognostic value of fluorescent subtype of phosphorus dendrimers to model cell distrubution of cationic dendritic vehicles for drugs and nucleic acids with different intracellular target regions.

Earlier efforts to develop optical sensors for macrophage polarization exploited the variation in expression levels of folate and mannose receptors, characteristic for M1 and M2 phenotypes, respectively.[66] Phenotype-specific spectral changes in phosphorus dendrimer emission profile suggest that this novel compound can serve as an indicator of subcellular events related to macrophage polarization physiology. Spectral shift in specific areas of dendrimer-loaded macrophages might be caused by differential binding of dendrimer molecules to cell proteins or other metabolites, changes in intramolecular charge transfer, or chemical changes in cytoplasmic compartments such as maturation or redistribution of acidic granules/endosomes in activated macrophages.[73] For instance, phagosomes of M1 macrophages were shown to differ significantly in proton-pumping activity compared to M2 phagosomes, resulting in distinct kinetics of acidification and maturation.[74] These chemical changes, oxidation, or enzyme activity may result in partial or complete degradation of the dendrimer, while its constituent fluorophore alone has an emission maximum of 485 nm, blue-shifted compared to the assembled dendrimer molecule maximum (Figure 1). In that case, the extent of spectral shift (Figure 4B) may indicate the degree to which the dendrimer is hydrolyzed. It remains to be determined whether the observed subcellular spectral variations can be reliably attributed to any specific physiological changes in activated macrophages, or be a marker of more general metabolic events, stress response, or cell status alterations. Beyond the dendrimer-fluorophore bio-imaging approach reported in this study, status-specific alteration of dendrimer structure may offer new avenues for targeted cargo release in dendrimer-based drug/nucleic acid delivery applications.

Our data on limited retention of dendrimer-labeled macrophages in sham injury as compared to contusion corroborate recent findings showing active exclusion of hematopoietic monocytes from the healthy CNS,[75] as well as other findings on reduced cell survival upon injection into the intact as opposed to injured CNS.[33] Several papers dating back to as early as 1990s[34,41] report the beneficial role of macrophages as a cell therapy tool for SCI.[34,35,42] Therapeutic use of pre-activated macrophages in combination with phosphorus dendrimer modifications possessing proven anti-inflammatory properties,[18,20,25] or loaded with therapeutic cargo,[21–23] may elicit synergistic regenerative effects in a variety of neurologic conditions.

The status of macrophage activation in the spinal cord depends on the environmental cues and the time course of neuroregenerative responses, with pro-inflammatory M1 polarization, characterized by an increased secretion of inflammatory and toxic mediators and elevated expression of co-stimulatory molecules,[44,76] prevailing in the first days after injury. Our time points for analysis were selected based on recent findings,[56] which showed the peak of classical hematogenous macrophage response to SCI at day 7 and high prevalence of a non-classical subset at day 14 (ref.[56]and Figure 3F therein). This allowed us to detect robust blue-shifted areas in a subset of implanted cells at week 1, linking the spectral properties of intracellular dendrimer after M1 activation in vitro to the microenvironment of inflamed spinal cord (Figure 7).

As the inflammation phase proceeds into regeneration and functional recovery, the SCI environment becomes dominated by macrophages with alternative (M2) activation status, associated with anti-inflammatory phenotype and secretion profile.[77] Indeed, the switch of macrophage phenotype from pro-inflammatory to intermediate/neuroprotective is associated with internalization of myelin debris,[65,71] which corresponds well with our observations on macrophages at the week 2 time point. Figure 6D shows myelin phagocytosis by representative dendrimer-loaded macrophages, in which M1-associated blue-shifted granules are no longer detectable. This intermediate/protective phenotype may have originated from the subset of initially implanted population which have assumed the non-classical pathway, with the M1 macrophages being removed after their function is no longer needed; or partly originated via the phenotypic conversion of M1-activated cells (which may imply some mechanisms for cell reorganization involving the disposal of the blue-shifted fluorophore). By week 2 after contusion injury macrophages reach their peak in myelin uptake,[78] associated with a switch to a protective phenotype,[56] and functional recovery from SCI is underway. Thus, subcellular spectral variations in dendrimer-loaded BM-derived macrophages appear to recapitulate the in vitro observations on pro-inflammatory and protective polarization at corresponding time points (inflammation and recovery phases) in SCI model.

© 2015 WILEY-VCH Verlag GmbH & Co. KGaA, Weinheim

16165195, 2015, 11, Downloaded from https://onlinelibrary.wiley.com/doi/10.1002/mabi.201500150 by Universidade De Madeira, Wiley Online Library on [28/02/2024]. See the Terms and Conditions (https://onlinelibrary.wiley.com/terms-and-conditions) on Wiley Online Library for rules of use; OA articles are governed by the applicable Creative Commons License

5. Conclusion

We have demonstrated that fluorescent phosphorus dendrimer is readily internalized and maintained by BM-derived macrophages, making it a useful cytoplasmic tracer in both in vitro and in vivo settings. Fluorescent dendrimers can be used to model and predict drug and RNA/DNA delivery and distribution in the cell by the cationic dendritic vehicles. Such studies could provide a rationale for the development of efficient and specific dendriplex-based vehicles, while robust and stable fluorescence will allow specific tracing of transfected cells to study their function and fate in vivo. Transplantation of dendrimer-labeled macrophages complements and supports the existing paradigms on retention and function of blood–borne phagocytes in spinal cord injury model. Sensitivity of dendrimer emission profile to the macrophage physiological status generates distinct spectral phenotypes likely linked to dendrimer structure alterations, a feature which may provide further insights into macrophage cell biology, offer new strategies for targeted release of therapeutic cargos, and assist in tracing macrophage plasticity in longitudinal studies in vitro and in vivo.

Acknowledgements: This research was supported by a grant from MS Scientific Foundation Canada, AI-HS, CRC, Leblanc Chair for Spinal Cord Research.

Received: April 29, 2015; Revised: May 29, 2015; Published online: July 14, 2015; DOI: 10.1002/mabi.201500150

Keywords: macrophage polarization; spinal cord injury; fluorescent phosphorus dendrimer; cell tracker; spectral shift

[1] T. R. Krishna, M. Parent, M. H. Werts, L. Moreaux, S. Gmouh, S. Charpak, A. M. Caminade, J. P. Majoral, M. Blanchard-Desce, *Angew Chem. Int. Ed. Engl.* **2006**, *45*, 4645.
[2] S. Mignani, K. S. El, M. Bousmina, J. P. Majoral, *Adv. Drug Deliv. Rev.* **2013**, *65*, 1316.
[3] S. Mignani, K. S. El, M. M. Bousmina, J. P. Majoral, *Chem. Rev.* **2014**, *114*, 1327.
[4] D. Shcharbin, A. Janaszewska, B. Klajnert-Maculewicz, B. Ziemba, V. Dzmitruk, I. Halets, S. Loznikova, N. Shcharbina, K. Milowska, M. Ionov, A. Shakhbazau, M. Bryszewska, *J. Control Release* **2014**, *181*, 40.
[5] L. Xu, H. Zhang, Y. Wu, *ACS. Chem. Neurosci.* **2014**, *5*, 2.
[6] J. L. Santos, H. Oliveira, D. Pandita, J. Rodrigues, A. P. Pego, P. L. Granja, H. Tomas, *J. Control Release* **2010**, *144*, 55.
[7] D. Shcharbin, A. Shakhbazau, M. Bryszewska, *Expert Opin. Drug Deliv.* **2013**, *10*, 1687.
[8] M. Guo, O. Varnavski, A. Narayanan, O. Mongin, J. P. Majoral, M. Blanchard-Desce, T. Goodson, *J. Phys. Chem. A* **2009**, *113*, 4763.
[9] O. Mongin, T. R. Krishna, M. H. Werts, A. M. Caminade, J. P. Majoral, M. Blanchard-Desce, *Chem. Commun. Camb.* **2006**, *8*, 915.
[10] W. Ke, K. Shao, R. Huang, L. Han, Y. Liu, J. Li, Y. Kuang, L. Ye, J. Lou, C. Jiang, *Biomaterials* **2009**, *30*, 6976.
[11] Y. Liu, R. Huang, L. Han, W. Ke, K. Shao, L. Ye, J. Lou, C. Jiang, *Biomaterials* **2009**, *30*, 4195.
[12] H. Dai, R. S. Navath, B. Balakrishnan, B. R. Guru, M. K. Mishra, R. Romero, R. M. Kannan, S. Kannan, *Nanomedicine Lond.* **2010**, *5*, 1317.
[13] S. Kannan, H. Dai, R. S. Navath, B. Balakrishnan, A. Jyoti, J. Janisse, R. Romero, R. M. Kannan, *Sci Transl Med.* **2012**, *4*, 130ra46.
[14] M. Hayder, M. Poupot, M. Baron, D. Nigon, C. O. Turrin, A. M. Caminade, J. P. Majoral, R. A. Eisenberg, J. J. Fournie, A. Cantagrel, R. Poupot, J. L. Davignon, *Sci. Transl. Med.* **2011**, *3*, 81ra35.
[15] K. Milowska, T. Gabryelak, M. Bryszewska, A. M. Caminade, J. P. Majoral, *Int. J. Biol. Macromol.* **2012**, *50*, 1138.
[16] T. Wasiak, M. Ionov, K. Nieznanski, H. Nieznanska, O. Klementieva, M. Granell, J. Cladera, J. P. Majoral, A. M. Caminade, B. Klajnert, *Mol. Pharm.* **2012**, *9*, 458.
[17] Y. Degboe, S. Fruchon, M. Baron, D. Nigon, C. O. Turrin, A. M. Caminade, R. Poupot, A. Cantagrel, J. L. Davignon, *Arthritis Res. Ther.* **2014**, *16*, R98.
[18] S. Fruchon, M. Poupot, L. Martinet, C. O. Turrin, J. P. Majoral, J. J. Fournie, A. M. Caminade, R. Poupot, *J. Leukoc. Biol.* **2009**, *85*, 553.
[19] M. Poupot, L. Griffe, P. Marchand, A. Maraval, O. Rolland, L. Martinet, F. E. L'Faqihi-Olive, C. O. Turrin, A. M. Caminade, J. J. Fournie, J. P. Majoral, R. Poupot, *FASEB J.* **2006**, *20*, 2339.
[20] S. Fruchon, A. M. Caminade, C. Abadie, J. L. Davignon, J. M. Combette, C. O. Turrin, R. Poupot, *Molecules* **2013**, *18*, 9305.
[21] V. Briz, M. J. Serramia, R. Madrid, A. Hameau, A. M. Caminade, J. P. Majoral, M. A. Munoz-Fernandez, *Curr. Med. Chem.* **2012**, *19*, 5044.
[22] A. V. Shakhbazau, D. G. Shcharbin, N. V. Goncharova, I. N. Seviaryn, S. M. Kosmacheva, N. A. Kartel, M. Bryszewska, J. P. Majoral, M. P. Potapnev, *Bull. Exp. Biol. Med.* **2011**, *151*, 126.
[23] D Shcharbin, V. Dzmitruk, A. Shakhbazau, N. Goncharova, I. Seviaryn, S. Kosmacheva, M. Potapnev, E. Pedziwiatr-Werbicka, M. Bryszewska, M. Talabaev, A. Chernov, V. Kulchitsky, A. M. Caminade, J. P. Majoral, *Pharmaceutics* **2011**, *3*, 458.
[24] B. Wang, R. S. Navath, A. R. Menjoge, B. Balakrishnan, R. Bellair, H. Dai, R. Romero, S. Kannan, R. M. Kannan, *Int. J. Pharm.* **2010**, *395*, 298.
[25] D. Portevin, M. Poupot, O. Rolland, C. O. Turrin, J. J. Fournie, J. P. Majoral, A. M. Caminade, R. Poupot, *J. Transl. Med.* **2009**, *7*, 82.
[26] E. Pedziwiatr-Werbicka, E. Fuentes, V. Dzmitruk, J. Sanchez-Nieves, M. Sudas, E. Drozd, A. Shakhbazau, D. Shcharbin, F. J. de la Mata, R. Gomez-Ramirez, M. A. Munoz-Fernandez, M. Bryszewska, *Colloids Surf B Biointerfaces* **2013**, *109*, 183.
[27] A. Shakhbazau, C. Mohanty, D. Shcharbin, M. Bryszewska, A. M. Caminade, J. P. Majoral, J. Alant, R. Midha, *J. Control Release* **2013**, *172*, 841.
[28] A. Shakhbazau, D. Shcharbin, M. Bryszewska, R. Kumar, H. M. Wobma, M. S. Kallos, N. Goncharova, I. Seviaryn, S. Kosmacheva, M. Potapnev, R. Midha, *Curr. Med. Chem.* **2012**, *19*, 5572.
[29] J. L. Santos, E. Oramas, A. P. Pego, P. L. Granja, H. Tomas, *J. Control Release* **2009**, *134*, 141.
[30] A. Shakhbazau, D. Shcharbin, N. Petyovka, N. Goncharova, I. Seviaryn, S. Kosmacheva, M. Bryszewska, M. Potapnev, *J. Pharm. Sci.* **2012**, *101*, 1546.
[31] A. Shakhbazau, D. Shcharbin, I. Seviaryn, N. Goncharova, S. Kosmacheva, M. Potapnev, M. Bryszewska, R. Kumar, J. Biernaskie, R. Midha, *Mol. Pharm.* **2012**, *9*, 1521.

© 2015 WILEY-VCH Verlag GmbH & Co. KGaA, Weinheim

[32] H. T. Khuong, R. Kumar, F. Senjaya, J. Grochmal, A. Ivanovic, A. Shakhbazau, J. Forden, A. Webb, J. Biernaskie, R. Midha, *Exp. Neurol.* **2014**, *254*, 168.
[33] G. Nikkhah, C. Rosenthal, G. Falkenstein, A. Roedter, A. Papazoglou, A. Brandis, *Cell Transplant.* **2009**, *18*, 119.
[34] O. Rapalino, O. Lazarov-Spiegler, E. Agranov, G. J. Velan, E. Yoles, M. Fraidakis, A. Solomon, R. Gepstein, A. Katz, M. Belkin, M. Hadani, M. Schwartz, *Nat. Med.* **1998**, *4*, 814.
[35] M. Schwartz, E. Yoles, *J. Neurotrauma.* **2006**, *23*, 360.
[36] A. Shakhbazau, C. Mohanty, R. Kumar, R. Midha, *J. Neurosurg.* **2014**, *121*, 423.
[37] J. A. Biernaskie, I. A. McKenzie, J. G. Toma, F. D. Miller, *Nat. Protoc.* **2006**, *1*, 2803.
[38] I. A. McKenzie, J. Biernaskie, J. G. Toma, R. Midha, F. D. Miller, *J. Neurosci.* **2006**, *26*, 6651.
[39] A. V. Shakhbazau, N. V. Goncharova, S. M. Kosmacheva, N. A. Kartel', M. P. Potapnev, *Bull. Exp. Biol. Med.* **2009**, *147*, 513.
[40] A. V. Shakhbazau, N. V. Petyovka, S. M. Kosmacheva, M. P. Potapnev, *Bull. Exp. Biol. Med.* **2011**, *150*, 547.
[41] N. Knoller, G. Auerbach, V. Fulga, G. Zelig, J. Attias, R. Bakimer, J. B. Marder, E. Yoles, M. Belkin, M. Schwartz, M. Hadani, *J. Neurosurg. Spine* **2005**, *3*, 173.
[42] M. Schwartz, E. Yoles, *Acta Neurochir. Suppl.* **2005**, *93*, 147.
[43] Y. Bomstein, J. B. Marder, K. Vitner, I. Smirnov, G. Lisaey, O. Butovsky, V. Fulga, E. Yoles, *J. Neuroimmunol.* **2003**, *142*, 10.
[44] J. F. Bogie, P. Stinissen, J. J. Hendriks, *Acta Neuropathol.* **2014**, *128*, 191.
[45] M. Zattoni, M. L. Mura, F. Deprez, R. A. Schwendener, B. Engelhardt, K. Frei, J. M. Fritschy, *J. Neurosci.* **2011**, *31*, 4037.
[46] A. R. Simard, D. Soulet, G. Gowing, J. P. Julien, S. Rivest, *Neuron* **2006**, *49*, 489.
[47] N. C. Derecki, J. C. Cronk, Z. Lu, E. Xu, S. B. Abbott, P. G. Guyenet, J. Kipnis, *Nature* **2012**, *484*, 105.
[48] M. Asheuer, F. Pflumio, S. Benhamida, A. Dubart-Kupperschmitt, F. Fouquet, Y. Imai, P. Aubourg, N. Cartier, *Proc. Natl. Acad. Sci. U S A.* **2004**, *101*, 3557.
[49] A. Biffi, P. M. De, A. Quattrini, C. U. Del, S. Amadio, I. Visigalli, M. Sessa, S. Fasano, R. Brambilla, S. Marchesini, C. Bordignon, L. Naldini, *J Clin Invest.* **2004**, *113*, 1118.
[50] W. J. Krall, P. M. Challita, L. S. Perlmutter, D. C. Skelton, D. B. Kohn, *Blood* **1994**, *83*, 2737.
[51] B. Ajami, J. L. Bennett, C. Krieger, K. M. McNagny, F. M. Rossi, *Nat. Neurosci.* **2011**, *14*, 1142.
[52] V. W. Yong, S. Rivest, *Neuron* **2009**, *64*, 55.
[53] S. Gordon, *Nat. Rev. Immunol.* **2003**, *3*, 23.
[54] D. M. Mosser, *Nat. Rev. Immunol.* **2008**, *8*, 958.
[55] P. J. Murray, T. A. Wynn, *Nat. Rev. Immunol.* **2011**, *11*, 723.
[56] S. G. Thawer, L. Mawhinney, K. Chadwick, S. N. de Chickera, L. C. Weaver, A. Brown, G. A. Dekaban, *J Neuroimmunol* **2013**, *261*, 7.
[57] K. L. Wong, W. H. Yeap, J. J. Tai, S. M. Ong, T. M. Dang, S. C. Wong, *Immunol. Res.* **2012**, *53*, 41.
[58] A. Mantovani, S. K. Biswas, M. R. Galdiero, A. Sica, M. Locati, *J. Pathol.* **2013**, *229*, 176.
[59] M. R. Kotter, W. W. Li, C. Zhao, R. J. Franklin, *J. Neurosci.* **2006**, *26*, 328.
[60] Z. M. van, J. N. Samsom, E. E. Nieuwenhuis, M. J. Melief, A. F. Wierenga-Wolf, I. E. Dijke, S. Talens, M. M. van, J. S. Voerman, L. A. Boven, J. D. Laman, *J Leukoc Biol.* **2011**, *90*, 123.
[61] B. Ajami, J. L. Bennett, C. Krieger, W. Tetzlaff, F. M. Rossi, *Nat. Neurosci.* **2007**, *10*, 1538.
[62] N. Ghasemlou, D. Bouhy, J. Yang, R. Lopez-Vales, M. Haber, T. Thuraisingam, G. He, D. Radzioch, A. Ding, S. David, *Brain* **2010**, *133*, 126.
[63] O. Mongin, L. Porres, M. Charlot, C. Katan, M. Blanchard-Desce, *Chemistry* **2007**, *13*, 1481.
[64] A. J. Fleetwood, H. Dinh, A. D. Cook, P. J. Hertzog, J. A. Hamilton, *J. Leukoc. Biol.* **2009**, *86*, 411.
[65] L. A. Boven, M. M. van, Z. M. van, A. Wierenga-Wolf, R. Q. Hintzen, R. G. Boot, J. M. Aerts, S. Amor, E. E. Nieuwenhuis, J. D. Laman, *Brain.* **2006**, *129*, 517.
[66] D. W. Baker, J. Zhou, Y. T. Tsai, K. M. Patty, H. Weng, E. N. Tang, A. Nair, W. J. Hu, L. Tang, *Acta Biomater.* **2014**, *10*, 2945.
[67] A. Shakhbazau, J. A. Martinez, Q. G. Xu, J. Kawasoe, M. J. van, R. Midha, *J. Neurochem.* **2012**, *122*, 501.
[68] J. D. Tario, Jr., K. Humphrey, A. D. Bantly, K. A. Muirhead, J. S. Moore, P. K. Wallace, *J. Vis. Exp.* **2012**, e4287
[69] V. S. Talanov, C. A. Regino, H. Kobayashi, M. Bernardo, P. L. Choyke, M. W. Brechbiel, *Nano Lett.* **2006**, *6*, 1459.
[70] H. Yan, L. Wang, J. Wang, X. Weng, H. Lei, X. Wang, L. Jiang, J. Zhu, W. Lu, X. Wei, C. Li, *ACS. Nano* **2012**, *6*, 410.
[71] C. M. Lamy, O. Sallin, C. Loussert, J. Y. Chatton, *ACS. Nano* **2012**, *6*, 1176.
[72] S. K. Choi, M. Verma, J. Silpe, R. E. Moody, K. Tang, J. J. Hanson, J. R. Baker, Jr., *Bioorg. Med. Chem.* **2012**, *20*, 1281.
[73] J. Canton, *J. Leukoc. Biol.* **2014**, *98*, 729.
[74] J. Canton, R. Khezri, M. Glogauer, S. Grinstein, *Mol. Biol. Cell* **2014**, *25*, 3330.
[75] F. Ginhoux, M. Greter, M. Leboeuf, S. Nandi, P. See, S. Gokhan, M. F. Mehler, S. J. Conway, L. G. Ng, E. R. Stanley, I. M. Samokhvalov, M. Merad, *Science.* **2010**, *330*, 841.
[76] J. J. Hendriks, C. E. Teunissen, H. E. de Vries, C. D. Dijkstra, *Brain Res. Brain Res. Rev.* **2005**, *48*, 185.
[77] R. Shechter, M. Schwartz, *J. Pathol.* **2013**, *229*, 332.
[78] A. D. Greenhalgh, S. David, *J. Neurosci.* **2014**, *34*, 6316.

© 2015 WILEY-VCH Verlag GmbH & Co. KGaA, Weinheim

16165195, 2015, 11, Downloaded from https://onlinelibrary.wiley.com/doi/10.1002/mabi.201500150 by Universidade De Madeira, Wiley Online Library on [28/02/2024]. See the Terms and Conditions (https://onlinelibrary.wiley.com/terms-and-conditions) on Wiley Online Library for rules of use; OA articles are governed by the applicable Creative Commons License